# Attosecond electronic dynamics of core-excited states of N<sub>2</sub>O in the soft x-ray region

Nariyuki Saito, <sup>1,\*</sup> Nicolas Douguet, <sup>2</sup> Hiroki Sannohe, <sup>1</sup> Nobuhisa Ishii <sup>0,3</sup> Teruto Kanai, <sup>1</sup> Yi Wu, <sup>4</sup> Andrew Chew, <sup>4</sup> Seunghwoi Han, <sup>4,5</sup> Barry I. Schneider, <sup>6</sup> Jeppe Olsen, <sup>7</sup> Luca Argenti, <sup>4</sup> Zenghu Chang <sup>0,4</sup> and Jiro Itatani <sup>0,1,†</sup> 

<sup>1</sup> The Institute for Solid State Physics, The University of Tokyo, 5-1-5 Kashiwanoha, Kashiwa, Chiba 277-8581, Japan 

<sup>2</sup> Kennesaw State University, Marietta, Georgia 30060, USA

<sup>3</sup> Kansai Photon Science Institute, National Institutes for Quantum and Radiological Science and Technology, 

8-1-7 Umemidai, Kizugawa, Kyoto 619-0215, Japan

<sup>4</sup> CREOL and Department of Physics, University of Central Florida, 4111 Libra Drive, PS430, Orlando, Florida 32816, USA 

<sup>5</sup> School of Mechanical Engineering, Chonnam National University, 77 Yongbong-ro, Buk-gu, Gwangju 61186, South Korea 

<sup>6</sup> National Institute of Standards and Technology, Gaithersburg, Maryland 20899, USA 

<sup>7</sup> Department of Chemistry, qLEAP Center for Theoretical Chemistry, Aarhus University, Langelandsgade 140, DK-8000 Aarhus C, Denmark

(Received 28 August 2021; accepted 17 November 2021; published 27 December 2021)

We present a combined experimental and theoretical study of the transient absorption spectroscopy of  $N_2O$  at the N K edge (400 eV) by employing an attosecond soft x-ray pulse and an overlapping intense femtosecond infrared pulse. Our experiment demonstrates that tunnel ionization of the core-excited states of neutral  $N_2O$  causes prominent half-cycle oscillations in the absorption signal. In addition, we observe the appearance of the  $N_2O^+$  signal with increasing delay as a result of the tunneling ionization of  $N_2O$ , thereby allowing us to follow the tunneling process in real time. We have developed theoretical models that allow us to interpret and reproduce the main trends of the experimental data.

DOI: 10.1103/PhysRevResearch.3.043222

## I. INTRODUCTION

The creation of core-excited states is a fundamental process in x-ray-matter interactions. The lifetime of core-excited states, especially above the soft x-ray (SX) region (>250 eV), is typically a few femtoseconds. This brevity is due to fast relaxation processes such as Auger decay. These short timescales make it difficult to probe the real-time dynamics of core-excited states with conventional SX sources such as synchrotron radiation. On the other hand, research in attosecond spectroscopy based on high-harmonic generation (HHG) has successfully shown the real-time dynamics of valence- and core-excited states in the extreme ultraviolet (XUV) region (10–250 eV) via photoelectron [1] and transient absorption spectroscopy (TAS) [2–6]. Recent advances in infrared (IR) to mid-IR ultrafast laser technology have pushed the cutoff energy of the high harmonics (HHs) into the SX region [7–12]. By using the HHs in the SX region, femtosecond pump-probe spectroscopy can trace chemical dynamics [13,14]. Although attosecond SX spectroscopy offers a way to access the dynamics of the core-excited states at their natural timescales,

Published by the American Physical Society under the terms of the Creative Commons Attribution 4.0 International license. Further distribution of this work must maintain attribution to the author(s) and the published article's title, journal citation, and DOI.

it still represents a technological challenge with only few experiments having been reported to date [15–17].

In this paper, we report on attosecond TAS of N<sub>2</sub>O molecules using femtosecond IR pulses and attosecond SX pulses at the N K edge (400 eV). The measured transient absorption spectra show two main features: (i) modulation of the SX absorption with a period that is one half-cycle of the IR field, and (ii) monotonic increase and decrease of the SX absorption due to the tunnel ionization of neutral N<sub>2</sub>O in the ground state. We perform theoretical simulations to successfully reproduce these features. Furthermore, the simulations show that the origin of the half-cycle oscillations is the tunnel ionization of the core-excited states. This mechanism is different from previously reported XUV TAS studies that attribute the origin of the half-cycle oscillations to laser-induced coupling among discrete electronic states [2–4] or the groundstate polarization effect that is driven by strong laser fields [19]. Our mechanism explains the half-cycle oscillations in a similar manner to the mechanism reported in the paper on the SX TAS of Ar [15]. We use a simple theoretical dipole model to develop an intuitive picture of this mechanism and find that the tunneling-induced modulation of the transition dipole between the core-excited and ground states causes the half-cycle oscillations. Our results indicate that the real-time dynamics of the core-excited states in the tunneling regime can be retrieved with attosecond precision by using SX TAS.

In the next section, we present our experimental setup and the results of the TAS measurements. In Sec. III, we apply a consistent theoretical framework which takes account of the combined dipole response of  $N_2O$  and  $N_2O^+$  produced by

<sup>\*</sup>Corresponding author: toshincompos@gmail.com †Corresponding author: jitatani@issp.u-tokyo.ac.jp

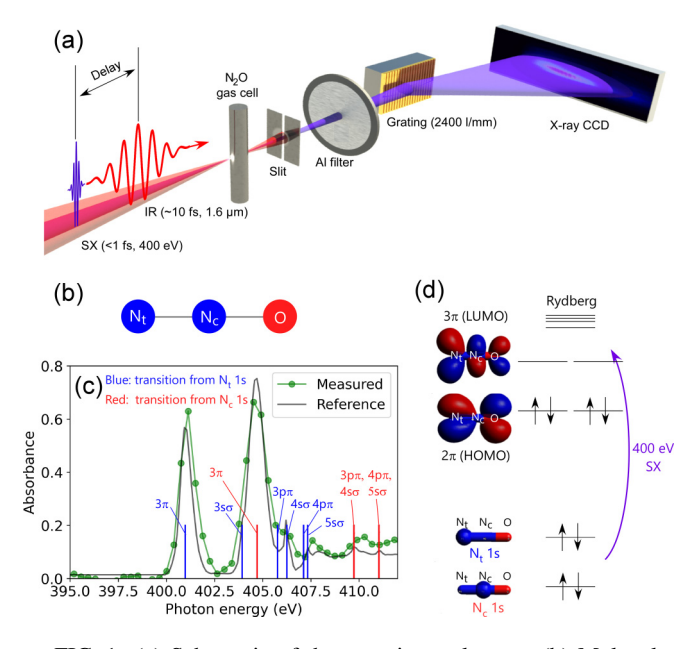


FIG. 1. (a) Schematic of the experimental setup. (b) Molecular geometry of  $N_2O$ . (c) Measured (green circles) and reference [18] (gray curve) absorption spectrum of  $N_2O$  at the N K edge; the blue and red lines represent the theoretical assignments [18] of the absorption peaks corresponding to the excitation of the  $N_t$  1s electron and the  $N_c$  1s electron, respectively. (d) Molecular orbital diagram of  $N_2O$ . HOMO, highest occupied molecular orbital; LUMO, lowest unoccupied molecular orbital.

tunnel ionization of  $N_2O$  in the intense laser field. This approach allows us to interpret and reproduce the main trends of the experimental spectrum, which is confirmed by the application of a simple dipole model. Finally, Sec. IV is devoted to our conclusions. Atomic units are used throughout the paper.

#### II. EXPERIMENTAL SETUP AND DATA

In the experiment, we employ a BiB<sub>3</sub>O<sub>6</sub>-based optical parametric chirped-pulse amplifier with a center wavelength of 1600 nm, pulse duration of 10 fs, pulse energy of 1.5 mJ, and repetition rate of 1 kHz [9] as a drive laser for HHG and TAS. The carrier-envelope phase (CEP) of the drive laser is passively stabilized. The schematic of the TAS setup is depicted in Fig. 1(a). The SX probe pulses are obtained by HHG in a gas cell filled with He at 3.05 bar. Generation of isolated attosecond SX pulses is confirmed by measuring the half-cycle cutoff that appears as CEP dependence in the SX spectra [20]. A portion of the drive laser is used as a pump pulse for the TAS measurement. The IR pump pulse and the SX probe pulse are linearly polarized in the same direction, and collinearly focused into a 1.5-mm-thick gas cell filled with N<sub>2</sub>O at 0.1 bar. The transmitted SX spectrum is resolved by a SX spectrometer consisting of a 50-\mu m-wide slit, a 150-nm-thick Al filter, a variable-line-spacing flat-field grating (Shimadzu 30-003, 2400 grooves/mm), and an x-ray CCD (ANDOR Newton SO). The delay between the pump and the probe pulses is scanned by a piezo stage. By using an interferometric feedback control system, a delay stability below 100 as is achieved.

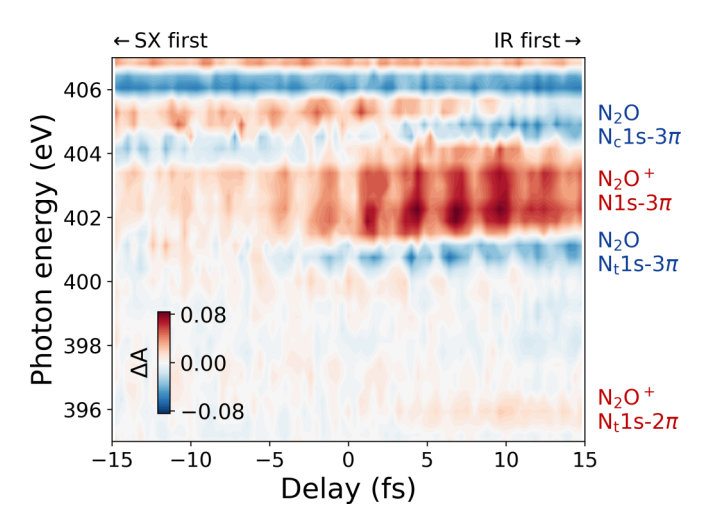


FIG. 2. Measured transient absorption spectra of  $N_2O$  at the N K edge. The positive delay indicates that the IR pulses arrive earlier than the SX pulses. The transitions of corresponding absorption peaks are shown on the right side of the figure.

Figure 1(b) illustrates the geometry of the  $N_2O$  molecule, with the central and terminal N atoms labeled N<sub>c</sub> and N<sub>t</sub>, respectively. The static absorption spectrum of N<sub>2</sub>O at the N K edge is shown in Fig. 1(c). The green circles represent data measured by our experimental setup, and the gray curve represents reference data measured using a synchrotron source [18]. The two large peaks at  $\sim$ 401 and  $\sim$ 405 eV correspond, respectively, to the excitation of an electron from the N<sub>t</sub> 1s or N<sub>c</sub> 1s core orbital to the  $3\pi$  orbital. As shown in the molecular orbital diagram in Fig. 1(d), the orbital energy of N<sub>c</sub> 1s is below that of N<sub>t</sub> 1s, which produces the double peak structure in the absorption spectrum. Figure 2 shows the measured transient absorption spectra of N<sub>2</sub>O at the N K edge as a function of the pump-probe delay. The location of time zero is determined by the rapid increase of absorption by N<sub>2</sub>O<sup>+</sup> N 1s-3 $\pi$  (~403 eV) with uncertainty of several femtoseconds. The absorbance at the  $N_2O$   $N_t$  1s-3 $\pi$ ( $\sim$ 401 eV) and at the N<sub>2</sub>O N<sub>c</sub> 1s-3 $\pi$  ( $\sim$ 405 eV) decreases at positive delays, while the absorbance between 401 and 405 eV increases. Our theoretical calculations, which are described in the next section, attribute this absorbance increase to the  $N_2O^+$   $N_t$  1s-3 $\pi$  and  $N_2O^+$   $N_c$  1s-3 $\pi$  transitions at  $\sim$ 402 and  $\sim$ 403 eV, respectively, which originate from the tunnel ionization of the N<sub>2</sub>O ground state that is induced by the IR pulse. Here, the ionization fraction is estimated to be around 20% based on the decrease of the absorption at the  $N_2O$   $N_t$  1s-3 $\pi$ and the  $N_2O$   $N_c$  1s-3 $\pi$  peaks in TAS data at longer delays, where the half-cycle oscillations become absent. On top of the monotonic increase and decrease of the absorbance, the experimental spectra exhibit prominent vertical fringes at half the period of the pump IR pulse ( $T_{\rm IR}/2 \sim 2.7$  fs) in both N<sub>2</sub>O and  $N_2O^+$  peaks.

#### III. THEORETICAL APPROACH

## A. Quantum chemistry calculations

The static electronic properties of the  $N_2O/N_2O^+$  valence and core-excited states are calculated at  $N_2O$  equilibrium

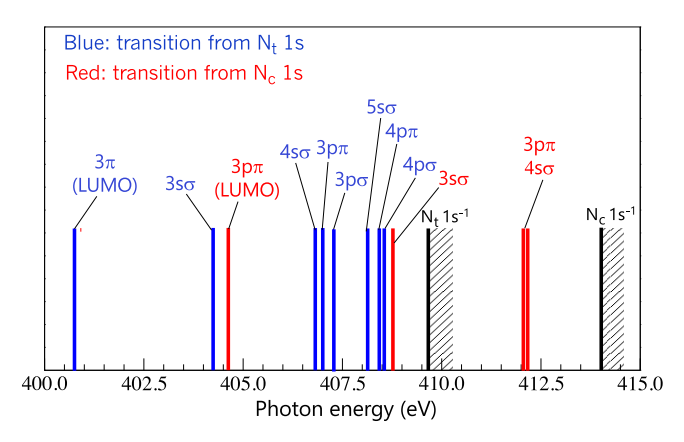


FIG. 3. Computed excitation energies of the various core-excited states of  $N_2O$  labeled with excitation from either the  $N_t$  or  $N_c$  1s orbital. The thick black lines with shaded areas indicate the  $N_t$  1s<sup>-1</sup> and  $N_c$  1s<sup>-1</sup> thresholds.

geometry using the MESA [21] quantum chemistry package. We start with the computation of N<sub>2</sub>O Hartree-Fock molecular orbitals (MOs) and use the correlation-consistent polarized valence triple-zeta (cc-pVTZ) [22] basis set for N and O, as well as diffuse s and p orbitals with exponents 0.015 and 0.003 to improve the description of Rydberg states. Next, we perform multireference configuration-interaction (MRCI) calculations to describe the core-hole orbitals, where we include all single and double excitations from the reference space, forcing a hole in either the N<sub>t</sub> or the N<sub>c</sub> 1s core orbital. These calculations are used to compute averaged natural orbitals (NOs) between the computed  $N_t$  and  $N_c$  1s core-hole states. This set of NOs is used to compute the N2O ground state and core-excited states using MRCI calculations including all single excitations out of the reference space, and double excitation only in the first two unoccupied MOs. Because the latter calculations also include configurations associated with valence excitations of  $N_2O$ , they require the computation of more than 100 roots (space size  $\sim$ 200 000 configuration state functions) to access all core-excited states involved in the experiment.

Although we use core orbitals optimized for the ions, we still obtained a good description of the  $N_2O$  ground state. In particular, we obtained excitation energies to coreexcited states in excellent agreement with data in the literature, e.g., we found  $N_t$  1s-3 $\pi$  and  $N_c$  1s-3 $\pi$  excitation energies of 400.80 and 404.67 eV, respectively. The positions of the calculated core-hole state transitions from the  $N_2O$  ground state are shown in Fig. 3. All transition dipole moments are then calculated from the MRCI calculations.

The calculation of  $N_2O^+$  electronic states is similar. We also start from  $N_2O$  Hartree-Fock MOs and compute NOs on core-hole excited states of  $N_2O^+$ . In this case, we have also found excitation energies for  $N_t$  1s-2 $\pi$  and N 1s-3 $\pi$  from the  $N_2O^+$  ground state to be in good agreement with our experimental data. The relative positions of all the relevant autoionizing states are in excellent agreement with the existing values in the literature [18,23], even without accounting

ab initio for the coupling of these states to the electronic continuum.

#### **B.** Time-dependent simulations

#### 1. Theoretical description of N<sub>2</sub>O TAS

The time-dependent simulations are performed by numerically integrating the time-dependent Schrödinger equation (TDSE),  $i\partial_t |\Psi(t)\rangle = H(t)|\Psi(t)\rangle$ , for the multielectron wave function  $|\Psi(t)\rangle$  of the neutral molecule, in a basis of discrete electronic states. The Hamiltonian  $H(t) = H_0 + H_I(t)$ is composed of the field-free Hamiltonian  $H_0$ , and the fieldmolecule interaction in the dipole approximation,  $H_I(t) =$  $-\vec{E}(t) \cdot \vec{\mu}_{el}$ , where  $\vec{E}(t) = \vec{E}_{SX}(t) + \vec{E}_{IR}(t)$  is the linearly polarized electric field and  $\vec{\mu}_{el}$  is the dipole operator in the length gauge. In the basis of electronic states,  $[H_0]_{ij}$  =  $\delta_{ii}[E_i - i\Gamma_a/2]$ , where  $\Gamma_a = 100$  meV is a phenomenological width introduced to model the autoionizing decay of all core-excited states, while the transition dipole moments between electronic states,  $[\vec{\mu}_{el}]_{ij}$ , are obtained using MESA [21]. The TDSE is propagated by splitting the time-evolution operator as  $\exp[-iH(t)dt] = \exp[-iH_0dt/2] \exp[-iH_I(t +$ dt/2)dt] exp[ $-iH_0dt/2$ ], and the dipole response,  $\vec{\mu}_{el}(t;\tau) =$  $\langle \Psi(t) | \vec{\mu}_{el} | \Psi(t) \rangle$ , is monitored over time. The optical density (OD) for a single fixed-in-space molecule aligned along  $\hat{z}$ and a field with a given polarization vector  $\hat{\varepsilon}$  is obtained as  $OD(\varepsilon; \omega, \tau) = \frac{4\pi}{\omega} Im[\bar{\mu}_{el}(\varepsilon; \omega, \tau)/\bar{E}_{SX}(\omega)]$ , where  $\omega$  is the light frequency, while  $\bar{\mu}_{el}(\varepsilon;\omega,\tau)$  and  $\bar{E}_{SX}(\omega)$  are the Fourier transform of  $\vec{\mu}_{el}(t, \tau) \cdot \hat{\varepsilon}$  and  $E_{SX}(t)$ , respectively.

In solving the TDSE, we first consider process I in Fig. 4(a). In this process, the SX pulse excites an electron in the N 1s core orbital to a valence orbital. Then the IR pulse subsequently promotes the electron to another valence orbital. The simulation comprises 18 electronic N<sub>2</sub>O states, including the ground state. In agreement with the experimental conditions, we employed a 300-as pump pulse with 400-eV central frequency and a 10-fs 1.6- $\mu$ m IR probe with an intensity of  $2 \times 10^{14}$  W/cm<sup>2</sup>. Figure 4(b) shows the numerical OD as a function of the delay, in the case of collinear SX and IR fields, polarized at  $\theta = 90^{\circ}$  with respect to the molecular axis to highlight the SX N 1s-3 $\pi$  transitions. If the dynamics is restricted to process I only, as the time delay increases, instead of featuring prominent oscillations the absorption gradually converges to the SX-only limit, in stark contrast with what is observed in the experiment. In particular, no core-hole dynamics between N<sub>c</sub> and N<sub>t</sub> is apparent from the spectrum, which can be explained with the two core-hole states being virtually decoupled.

The weakly bound core-hole states can also be directly ionized by the intense IR field [process II in Fig. 4(a)]. Since the Keldysh parameter is already as small as  $\gamma \approx 0.3$  for the  $3\pi$  core-hole states, the ionization process is well within the tunneling regime. To estimate the ionization rates of the various core-excited states, we use the atomic Ammosov-Delone-Krainov (ADK) theory [24], which is applicable for  $\gamma < 0.5$  and captures the essence of the tunneling mechanism, assuming zero initial angular momentum. With process II included, the core-excited states now acquire an instantaneous time-dependent width,  $\Gamma_i(t) = \Gamma_a + W_{\rm ADK}^i(t)$ , which will replace  $\Gamma_a$  in the Hamiltonian. Here, the ADK ionization rate is

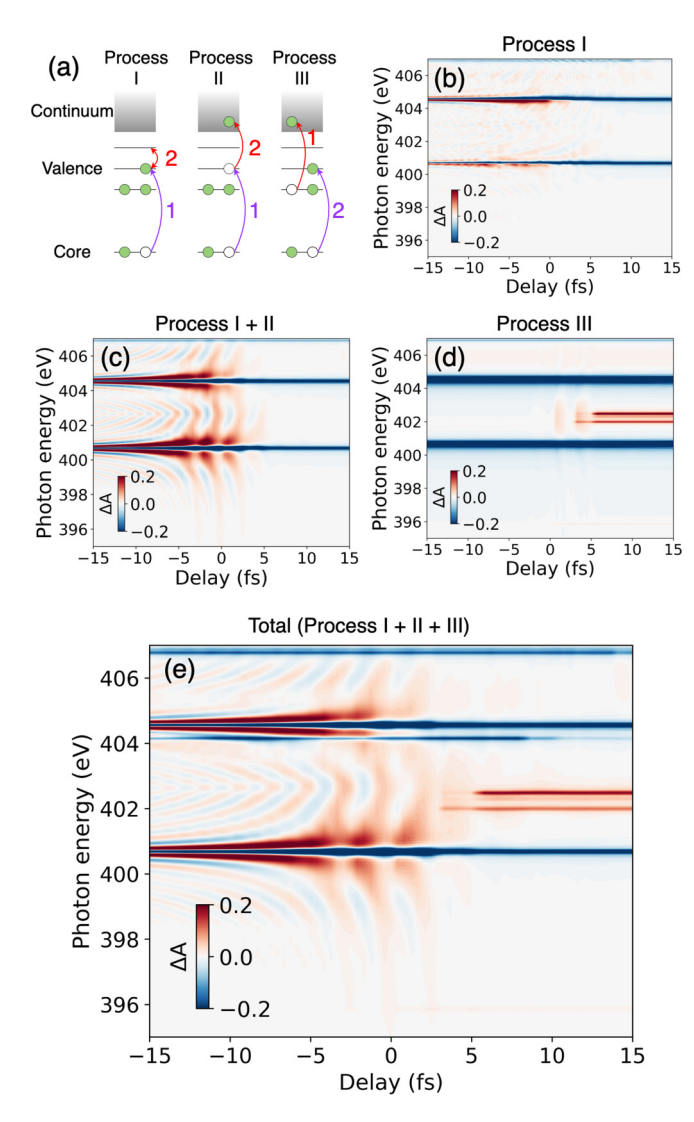


FIG. 4. (a) Schematic illustrations of the three theoretical processes considered in the TAS of  $N_2O/N_2O^+$ . Computed OD signal for linearly polarized light perpendicular to the molecular axis for (b) process I, (c) process I + II, and (d) process III (see text for details). (e) Computed OD signal which considers all the processes in (a) for randomly oriented molecules.

given by

$$W_{\text{ADK}}^{i}(t) = \frac{C_{p} 2^{2n^{*}} I_{p} e^{-\frac{2E_{0}}{3E_{\text{IR}}(t)}}}{n^{*} \Gamma(n^{*} + 1) \Gamma(n^{*})} \left(\frac{2E_{0}}{E_{\text{IR}}(t)}\right)^{2n^{*} - 1}.$$
 (1)

In Eq. (1), the ionization potential  $I_p = E_{th} - E_i$  of a core-excited state with energy  $E_i$  is taken from the parent ion threshold energy  $E_{th}$ ,  $n^* = \sqrt{2I_p}$  is the effective principal quantum number,  $C_p$  is a parameter common to all the core-excited states set to best reproduce the experimental spectrum, and  $E_0$  is the maximum field strength. The results of the delay scan for process I + II, presented in Fig. 4(c), reproduce the prominent half-cycle oscillations visible in the experiment. On the other hand, in the experimental data of Fig. 2, the hyperbolic fringes are difficult to see, which is caused by the energy resolution of the spectrometer being  $\sim 1.5$  eV.

## 2. Simple dipole model to explain the half-cycle oscillations

To understand the underpinning physics of the half-cycle oscillations in TAS, we create a simple dipole model which is closely related to the concept of free induction decay [5,25]. In this model, the temporal evolution of the dipole between the ground state and the core-excited state at a time t and a delay  $\tau$  is approximated as

$$d(t,\tau) \propto ie^{i\omega_{\rm ex}t}e^{-t/\tau_{\rm ex}}\sqrt{1-P_{\rm tunnel}(t,\tau)},$$
 (2)

where  $\omega_{\rm ex}$  is the energy difference between the ground state and the core-excited state,  $\tau_{\rm ex}$  is the natural lifetime of the core-excited state, and  $P_{\rm tunnel}(t,\tau)$  is the tunnel ionization probability of the core-excited state. The SX pulse is modeled as the delta function, and the time origin of t is defined by the arrival of the SX pulse. We calculate  $P_{\rm tunnel}(t,\tau)$  using the ADK model,

$$P_{\text{tunnel}}(t,\tau) = 1 - \exp\left(-\int_0^t dt' W_{\text{ADK}}^i [E_{\text{IR}}(t'+\tau)]\right), \quad (3)$$

where  $W_{\rm ADK}^i$  and  $E_{\rm IR}$  are the same as the ones used in the full theoretical simulation. The OD can be calculated from the dipole  $d(t,\tau)$  as  $\frac{4\pi}{\omega} {\rm Im}[\bar{d}(\omega,\tau)]$ , where  $\bar{d}(\omega,\tau)$  is the Fourier transform of  $d(t,\tau)$ .

The tunnel ionization rate as a function of time is shown in Fig. 5(a). It exhibits narrow peaks because the tunnel ionization is mostly confined near the IR intensity maxima. These ionization peaks cause periodic modulation of the dipole amplitude that strongly depends on the pump-probe delay, as shown in Fig. 5(b). The absorption spectrum is proportional to the Fourier transform of the dipole with respect to time. Since tunnel ionization rates peak with every half period of the IR pulse, the transient absorption spectra form beats with a half period of the IR fields. The above discussion is confirmed by the transient absorption spectrum in Fig. 5(c).

# 3. Theoretical description of N<sub>2</sub>O/N<sub>2</sub>O<sup>+</sup> TAS

We then consider process III in Fig. 4(a), in which the valence electron is tunnel ionized by the IR pulse to produce  $N_2O^+$ , and subsequently the core electron is excited to the valence orbitals by the SX pulse. A first-principles description of this process is challenging as it requires treating simultaneously two systems with different numbers of electrons. However, an approximate theoretical approach can be developed under the reasonable assumption that the formation of  $N_2O^+$  is only due to tunneling ionization from the  $N_2O$  ground state and that the process is irreversible. In these conditions, the TAS can be approximately described by the set of equations (see the Appendix for details)

$$i\partial_t |\Psi_P\rangle = H_{PP}(t)|\Psi_P\rangle - i\beta(t)|g\rangle c_g(t), \tag{4}$$

$$i\dot{\rho}_{ab} = [H'(t), \rho]_{ab} + i\delta_{ab}B_a(t)|c_g(t)|^2.$$
 (5)

In Eqs. (4) and (5),  $|\Psi\rangle$  is an N<sub>2</sub>O wave function that includes both bound and continuum states,  $|\Psi_P\rangle = P|\Psi\rangle$ , where P is the projector on N<sub>2</sub>O bound states,  $H_{PP}(t) = PH(t)P$ ,  $|g\rangle$  is the N<sub>2</sub>O ground state,  $c_g(t) = \langle g|\Psi\rangle$ ,  $\rho_{ab}$  is the element of the N<sub>2</sub>O<sup>+</sup> density matrix between ionic states a and b, and H(t) and H'(t) are the Hamiltonians of N<sub>2</sub>O and N<sub>2</sub>O<sup>+</sup>, respectively. The coefficient  $B_a(t) = 2|\alpha_a(t)|^2/\Gamma_a$  is the (positive)

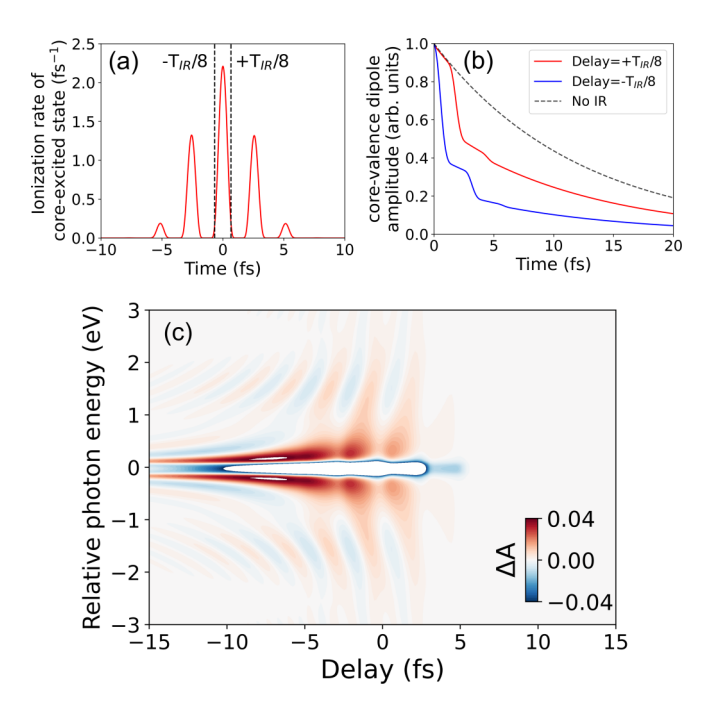


FIG. 5. Intuitive explanation of the mechanism of the half-cycle oscillations by the simple dipole model. (a) ADK ionization rate of the core-excited state used in the simple dipole model simulation. (b) Temporal evolution of the amplitude of the dipole between the ground state and the core-excited state. The red solid curve and the blue solid curve represent the cases when the IR pulse exists and the delay between the IR and the SX pulses is set to  $+T_{\rm IR}/8$  and  $-T_{\rm IR}/8$  ( $T_{\rm IR}$  is the period of the IR field), respectively. The black dashed curve represents the case when the IR pulse does not exist. (c) The transient absorption spectra obtained from the simple dipole model. The origin of the vertical axis is adjusted such that the photon energy of the absorption peak becomes zero when the IR is not present.

ionization rate to the ionic state a, where  $\Gamma_a$  is a characteristic tunneling width, and  $\alpha_a(t)$  is a transition-rate amplitude. This formalism meets the minimum requirement of preserving the total population.

Since in the condition of the current experiment, the ionization of the N<sub>2</sub>O ground state occurs almost exclusively from tunnel ionization of the HOMO molecular orbitals (see Fig. 1), we only consider the formation of N<sub>2</sub>O<sup>+</sup> in its degenerate  $\Pi$  ground state. The dependence of the tunneling rate on the light polarization is taken into account by introducing the rate amplitudes  $\alpha_{\parallel}$  and  $\alpha_{\perp}$  for the field parallel or perpendicular to the molecular axis, respectively. The ionization rate amplitudes of the  $2\pi_x$  and  $2\pi_y$  orbitals, for a field in the (xz) plane and a polarization angle  $\theta$ , are then approximated as  $\alpha_x^2(t) = \alpha_{\parallel}^2(t)\cos^2\theta + \alpha_{\perp}^2(t)\sin^2\theta$  and  $\alpha_y(t) = \alpha_{\parallel}(t)$ . Because the  $I_P$  of N<sub>2</sub>O is close to He<sup>+</sup> 2p orbital energy, we have set the ratio  $\alpha_{\parallel}^2/\alpha_{\perp}^2$  to match that of the ionization probability (obtained by solving the TDSE) for an IR field parallel or perpendicular to the  $2p_z$  orbital in He<sup>+</sup>.

The coupled equations (4) and (5) are solved numerically. The results, presented at  $\theta = 90^{\circ}$  in Fig. 4(d), show the appearance of the characteristic absorption lines of  $N_2O^+$  for positive delay. Once again, we observe half-cycle oscillations due to the tunneling ionization of the core-excited states of

N<sub>2</sub>O<sup>+</sup>. These features are clearly seen in the experimentally observed spectra in Fig. 2.

The final theoretical results in Fig. 4(e) include all the aforementioned processes and are averaged over the light polarization directions to reproduce the case of randomly oriented molecules. The empirical factor  $C_p$  in the tunneling rate of the  $N_2O$  ground state is chosen to reproduce the ionization fraction measured experimentally. All the main features of the experimental spectrum are well reproduced by the theoretical calculations. The remaining discrepancies can be attributed to possible experimental uncertainties and the necessary approximations introduced in our theoretical treatment. For instance, at a large positive delay (i.e., the IR-first case), the IR pulse can excite  $N_2O$  before core-hole excitation. This likely makes a non-negligible contribution that is not accounted for in our theoretical approach.

#### IV. CONCLUSIONS

In summary, we conduct attosecond TAS of N<sub>2</sub>O at the N K edge, which exhibits monotonic absorption changes due to creation of N<sub>2</sub>O<sup>+</sup> (process III) as well as half-cycle oscillations in the absorption lines of neutral N<sub>2</sub>O and ionic N<sub>2</sub>O<sup>+</sup> (processes II and III). Our TDSE-based simulations reproduce the experimental results by taking the three different processes into account. The simulation indicates that the dominant mechanism of the half-cycle oscillations is the tunnel ionization of the core-excited states. A simple dipole model shows that this mechanism can be understood as the sub-optical-cycle modulation of the electronic dipole amplitude between the ground state and the core-excited state due to tunnel ionization. Based on the above discussion, our method could, in principle, be extended to retrieve the time-dependent tunnel ionization rate [26], coherent electron dynamics [27], and charge migration [28] of core-excited states from transient absorption spectra. Finally, we remark that the difference between the dynamics of the  $N_t\ 1s$  and  $N_c\ 1s$  excited states could not be confirmed in this paper, possibly due to the limited energy resolution and the signal-to-noise ratio in the experiment. However, in the near future, we expect that further refined experimental and theoretical tools will allow us to distinguish the electronic dynamics of different core-excited states in a molecule, thus fully leveraging the element and site selectivity of SX absorption [29].

# ACKNOWLEDGMENTS

We are grateful to Dr. Kiyoshi Ueda for valuable suggestions. The experimental part of this work was funded by Grant-in-Aid for Scientific Research (S) No. 18H05250 of the Japan Society for the Promotion of Science, MEXT Quantum Leap Flagship Program (MEXT Q-LEAP) Grant No. JPMXS0118068681, U.S. Air Force Office of Scientific Research (AFOSR) Grant No. FA9550-20-1-0295, and the National Science Foundation (NSF) (Grant No. 1806575). The theoretical part was funded by the NSF under Grants No. PHY-1912507 (L.A.) and No. PHY-2012078 (N.D.). L.A. acknowledges support from DOE Career Grant No. DE-SC0020311.

## APPENDIX: FORMALISM DESCRIBING N2O/N2O+ TAS

In computing the TAS of the  $N_2O$  molecule, we are faced with the challenge of understanding a signal exhibiting features from both the neutral and the ionized molecules. To proceed, we begin with the assumption that generation of the ion is entirely due to tunnel ionization of the ground state of the neutral molecule. Even within this context, it is still not trivial to formulate a Schrödinger equation for both the neutral molecule and the ion that satisfies the principle of population conservation in the absence of tunneling from the ion itself. The present work is an attempt to derive such a model.

The TDSE for N<sub>2</sub>O interacting with an external field

$$i\partial_t |\Psi\rangle = H|\Psi\rangle$$
 (A1)

can be partitioned into a P space, consisting of the bound and excited states of the neutral molecule, and a Q space, containing the ionic states plus the photoejected electron with P + Q = I. The various states were computed using the MESA quantum chemistry package [21]. Then, we obtain

$$i\partial_t |\Psi_P\rangle = H_{PP} |\Psi_P\rangle + H_{PQ} |\Psi_Q\rangle,$$
  
$$i\partial_t |\Psi_Q\rangle = H_{QQ} |\Psi_Q\rangle + H_{QP} |\Psi_P\rangle,$$
 (A2)

where  $|\Psi_P\rangle = P|\Psi\rangle$ ,  $H_{PP} = PHP$ , etc. To model the tunnel ionization of the system, let us assume that  $H_{QP}$  can be written in the simple, separable form

$$H_{QP} = \sum_{a} |T_a\rangle\langle g| \ \alpha_a(t), \tag{A3}$$

where a labels the ionic state (tunnel ionization from different orbitals, such as  $\pi_x$  or  $\pi_y$ ),  $\alpha_a(t)$  is some positive ionization rate amplitude associated with the field and ion,  $|g\rangle$  is the ground state of the neutral molecule, and  $|T_a\rangle$  is the state of the system immediately after tunneling to ion a.  $T_a$  is taken to be not a simple stationary state, but an entangled state which is expressed as a broadband free-electron wave packet near the molecule,

$$|T_a\rangle = \int d\varepsilon |a\varepsilon\rangle \langle a\varepsilon|T_a\rangle, \quad \langle T_a|T_a\rangle = 1.$$
 (A4)

Within this simplifying assumption, the TDSE becomes

$$i\partial_{t}|\Psi_{P}\rangle = H_{PP}|\Psi_{P}\rangle + \sum_{a}\alpha_{a}(t)|g\rangle\langle T_{a}|\Psi_{Q}\rangle,$$

$$i\partial_{t}|\Psi_{Q}\rangle = H_{QQ}|\Psi_{Q}\rangle + \sum_{a}|T_{a}\rangle c_{g}(t)\alpha_{a}(t),$$
(A5)

where  $c_g(t)=\langle g|\Psi\rangle$ . To keep the model simple, it is useful to decouple the two equations. We proceed by assuming that  $\langle T_a|\Psi_Q\rangle$ , i.e., the overlap over time of the ion times photoelectron with the initial state immediately after the tunneling event, decays rapidly to zero. An estimate of the decay may be found by evaluating  $\langle T_a|\Psi_Q(t)\rangle$  in the absence of the external driving field;  $\langle T_a|\Psi_Q\rangle=\langle T_a|\Psi_Q^0\rangle$ , where  $|\Psi_Q^0\rangle$  is the solution in the case in which  $H_{QQ}(t)$  is replaced by its field-free component,  $H_{QQ}^0$ ,

$$i\partial_t |\Psi_Q^0\rangle = H_{QQ}^0 |\Psi_Q^0\rangle + \sum_a |T_a\rangle c_g(t)\alpha_a(t).$$
 (A6)

The equation

$$(i\partial_t - H_{OO}^0)|\Psi_{t'}\rangle = \delta(t - t')|\varphi\rangle, \quad |\Psi_{t'}(t < t')\rangle = 0, \quad (A7)$$

has the solution (retarded Green's function)

$$|\Psi_{t'}(t)\rangle = -i\theta(t - t')e^{-iH_{QQ}^0(t - t')}|\varphi\rangle. \tag{A8}$$

As a consequence,

$$\langle T_a | \Psi_Q \rangle = -i \int dt' \sum_b \langle T_a | e^{-iH_{QQ}^0(t-t')} | T_b \rangle c_g(t') \alpha_b(t'). \tag{AS}$$

The quantity  $\langle T_a|e^{-iH_{QQ}^0(t-t')}|T_b\rangle$  is the Fourier transform of the tunneled photoelectron spectrum,

$$\langle T_a | e^{-iH_{QQ}^0 t} | T_b \rangle = \delta_{ab} \int d\varepsilon |\langle a\varepsilon | T_a \rangle|^2 e^{-i\varepsilon t}. \tag{A10}$$

If the spectral width  $\Gamma_a$  of  $|T_a\rangle$  is much larger than the frequency  $\omega$  of the field that causes the tunneling, then  $\langle T_a|e^{-iH_{QQ}^0t}|T_a\rangle$  will decay on a much shorter timescale than the field period and, hopefully, more rapidly than any change in  $c_g(t)$  or  $\alpha_a(t)$  as well,

$$\langle T_a | \Psi_Q \rangle \simeq -i c_g(t) \alpha_a(t) \int dt' \langle T_a | e^{-iH_{QQ}^0(t-t')} | T_a \rangle$$
  
 $\simeq -i c_g(t) \alpha_a(t) / \Gamma_a.$  (A11)

Within these approximations, we can rewrite the TDSE for the neutral molecule and the ion as

$$i\partial_{t}|\Psi_{P}\rangle = H_{PP}|\Psi_{P}\rangle - i\sum_{a} \frac{|\alpha_{a}(t)|^{2}}{\Gamma_{a}}|g\rangle c_{g}(t),$$

$$i\partial_{t}|\Psi_{Q}\rangle = H_{QQ}|\Psi_{Q}\rangle + \sum_{a} |T_{a}\rangle c_{g}(t)\alpha_{a}(t). \tag{A12}$$

As expected, the dynamics of the neutral molecule can be described by a Schrödinger equation with an extinction term. For the states of the ion, however, we need to go one step further. At this point,  $|\Psi_Q\rangle$ , is an entangled state of the ion and the electron. To remove the dependence on the photoelectron, we require a master equation for the density matrix of the ion. Defining,  $a,b,c,\ldots$  as the states of the ion and  $\varepsilon_j$  as the states of the photoelectron,

$$|\Psi_{Q}(t)\rangle = \sum_{a} \sum_{j} |a\varepsilon_{j}\rangle c_{aj}(t).$$
 (A13)

The probability of detecting the photoelectron in the state j is  $P_j = \sum_a |c_{aj}|^2$ , and the residual state of the ion resulting from such measurement is  $|\Psi_j\rangle = \sum_a |a\rangle \, c_{aj}/\sqrt{P_j}$ . The density matrix for the ion, after the detachment of the photoelectron, is

$$\hat{\rho} = \sum_{j} |\Psi_{j}\rangle\langle\Psi_{j}|P_{j} = \sum_{ab} |a\rangle\langle b| \sum_{j} c_{aj} c_{bj}^{*}, \qquad (A14)$$

or  $\rho_{ab}=\sum_{j}c_{aj}c_{bj}^{*}.$  To derive an equation for  $\rho,$  we make the additional assumption

$$H_{QQ}(t) = H'(t) + h_e,$$
 (A15)

where H'(t) is the driven Hamiltonian of the ion and  $h_e$  is the field-free Hamiltonian for the photoelectron. The equation for

the coefficients  $c_{aj}$  is

$$i\dot{c}_{aj} = \sum_{b} H'_{ab}(t)c_{bj} + \varepsilon c_{aj} + \langle aj|T_a\rangle c_g\alpha_a.$$
 (A16)

The density matrix, then, satisfies the following equation:

$$i\dot{\rho}_{ab} = \sum_{j} i\dot{c}_{aj} c_{bj}^{*} - \sum_{j} c_{aj} (i\dot{c}_{bj})^{*}$$

$$= [H'(t), \rho]_{ab} + c_{g}\alpha_{a} \sum_{j} c_{bj}^{*} \langle aj|T_{a}\rangle$$

$$- c_{g}^{*}\alpha_{b} \sum_{j} \langle T_{b}|bj\rangle c_{aj}. \tag{A17}$$

To make progress, we need an estimate of

$$\sum_{j} \langle T_b | bj \rangle c_{aj} = \langle T_b | (|b\rangle \langle a| \otimes \hat{1}) | \Psi_Q \rangle, \tag{A18}$$

where  $\hat{1}$  is the identity over the photoelectron states. Proceeding with the reasonable assumption that the nondiagonal terms  $\langle T|(|b\rangle\langle a\neq b|\otimes \hat{1})|\Psi_Q\rangle$  are negligible compared with the diagonal terms,  $\langle T_a|\Psi_Q\rangle=-ic_g(t)\alpha_a(t)/\Gamma_a$ , yields

$$\sum_{i} \langle T_b | bj \rangle c_{aj} = -i \, \delta_{ab} \, c_g(t) \alpha_a(t) / \Gamma_a. \tag{A19}$$

Using the above results in a master equation for the ion,

$$i\dot{\rho}_{ab} = [H'(t), \rho]_{ab} + i\delta_{ab}|c_g|^2 \frac{2|\alpha_a|^2}{\Gamma_a}.$$
 (A20)

If we define  $\beta(t) = \sum_a \alpha_a^2(t)/\Gamma_a$  and  $B_a(t) = 2|\alpha_a|^2/\Gamma_a$ , where  $\sum_a B_a(t) = 2\beta(t)$ , the set of coupled equations for the neutral molecule and the ion may be cast in the form

$$i\partial_t \Psi_P = H_{PP} \Psi_P - i\beta(t)|g\rangle c_g(t),$$
  

$$i\dot{\rho}_{ab} = [H'(t), \rho]_{ab} + i\delta_{ab} B_a(t)|c_g(t)|^2.$$
 (A21)

The tunnel ionization rates from the  $\pi_x$  and  $\pi_y$  orbitals may be tentatively approximated as a function of the angle  $\theta$  of the

molecular axis with respect to the field polarization as

$$\alpha_{x}(t) = \sqrt{\alpha_{\parallel}^{2}(t)\cos^{2}\theta + \alpha_{\perp}^{2}(t)\sin^{2}\theta},$$

$$\alpha_{v}(t) = \alpha_{\parallel}(t).$$
(A22)

Note that this master equation for the ion is not equivalent to a Schrödinger equation for a pure state with a source term. In fact, a consistent treatment of the ion response is not possible within a purely coherent framework. Importantly, this formulation meets the minimal requirement of preserving the population,

$$\frac{d}{dt}\langle \Psi_P(t)|\Psi_P(t)\rangle = -2\beta(t)|c_g(t)|^2,$$

$$\frac{d}{dt}\sum \rho_{aa}(t) = 2\beta(t)|c_g(t)|^2.$$
(A23)

As usual, the TDSE for the neutral molecule can be solved separately. The population of the ground state,  $c_g(t)$ , is then used to compute the source term in the master equation for the ion. The master equation is still a linear equation for a vector in the Liouville space  $\{|a\rangle\langle b|\}$ ,

 $i\dot{\rho}_{ab} = \mathcal{L}_{ab,cd}(t)\rho_{cd} + i\delta_{ab}B_a(t)|c_g(t)|^2$ , (A24) with the initial condition  $\rho_{ab}(-\infty) = 0$ , where the Liouville operator  $\mathcal{L}(t)$  is given by

$$\mathcal{L}_{ab,cd}(t) = \delta_{bd} H'_{ac}(t) - H'_{db}(t) \delta_{ac}. \tag{A25}$$

If H(t) is Hermitian, so is  $\mathcal{L}$ ,

$$\mathcal{L}_{cd,ab}^{*}(t) = \mathcal{L}_{ab,cd}(t). \tag{A26}$$

As a consequence, the master equation for the ion ensemble can be solved with the same methodology as the TDSE, with the only noticeable difference being that the size of the space is the square of the number of ionic states, rather than the number of ionic states. However, the problem is still treatable if the number of ionic states is not too large. To compute the transient absorption, one needs access to the expectation values of the dipole in the neutral molecule and in the ion, which are given by the equations

$$\langle \vec{\mu} \rangle_{\text{neutral}}(t) = \langle \Psi_P(t) | \vec{\mu} | \Psi_P(t) \rangle,$$
 (A27)

$$\langle \vec{\mu} \rangle_{\text{ion}}(t) = \text{tr}[\vec{\mu}\hat{\rho}].$$
 (A28)

<sup>[1]</sup> M. Drescher, M. Hentschel, R. Kienberger, M. Uiberacker, V. Yakovlev, A. Scrinzi, Th. Westerwalbesloh, U. Kleineberg, U. Heinzmann, and F. Krausz, Time-resolved atomic inner-shell spectroscopy, Nature (London) 419, 803 (2002).

<sup>[2]</sup> M. Chini, X. Wang, Y. Cheng, Y. Wu, D. Zhao, D. A. Telnov, S.-I. Chu, and Z. Chang, Sub-cycle oscillations in virtual states brought to light, Sci. Rep. 3, 1105 (2013).

<sup>[3]</sup> C. Ott, A. Kaldun, L. Argenti, P. Raith, K. Meyer, M. Laux, Y. Zhang, A. Blattermann, S. Hagstotz, T. Ding, R. Heck, J. Madronero, F. Martin, and T. Pfeifer, Reconstruction and control of a time-dependent two-electron wave packet, Nature (London) 516, 374 (2014).

<sup>[4]</sup> Y. Kobayashi, H. Timmers, M. Sabbar, S. R. Leone, and D. M. Neumark, Attosecond transient-absorption dynamics of xenon

core-excited states in a strong driving field, Phys. Rev. A 95, 031401(R) (2017).

<sup>[5]</sup> H. Mashiko, T. Yamaguchi, K. Oguri, A. Suda, and H. Gotoh, Characterizing inner-shell with spectral phase interferometry for direct electric-field reconstruction, Nat. Commun. 5, 5599 (2014).

<sup>[6]</sup> A. Moulet, J. B. Bertrand, T. Klostermann, A. Guggenmos, N. Karpowicz, and E. Goulielmakis, Soft x-ray excitonics, Science 357, 1134 (2017).

<sup>[7]</sup> T. Popmintchev, M.-C. Chen, D. Popmintchev, P. Arpin, S. Brown, S. Ališauskas, G. Andriukaitis, T. Balčiunas, O. D. Mücke, A. Pugzlys, A. Baltuška, B. Shim, S. E. Schrauth, A. Gaeta, C. Hernández-García, L. Plaja, A. Becker, A. Jaron-Becker, M. M. Murnane, and H. C. Kapteyn, Bright coherent

- ultrahigh harmonics in the keV X-ray regime from mid-infrared femtosecond lasers, Science **336**, 1287 (2012).
- [8] S. L. Cousin, F. Silva, S. Teichmann, M. Hemmer, B. Buades, and J. Biegert, High-flux table-top soft x-ray source driven by sub-2-cycle, CEP stable, 1.85-μm 1-kHz pulses for carbon K-edge spectroscopy, Opt. Lett. 39, 5383 (2014).
- [9] N. Ishii, K. Kaneshima, T. Kanai, S. Watanabe, and J. Itatani, Generation of sub-two-cycle millijoule infrared pulses in an optical parametric chirped-pulse amplifier and their application to soft x-ray absorption spectroscopy with high-flux high harmonics, J. Opt. (Bristol) 20, 014003 (2017).
- [10] J. Li, X. Ren, Y. Yin, K. Zhao, A. Chew, Y. Cheng, E. Cunningham, Y. Wang, S. Hu, Y. Wu, M. Chini, and Z. Chang, 53-attosecond X-ray pulses reach the carbon K-edge, Nat. Commun. 8, 186 (2017).
- [11] A. S. Johnson, D. R. Austin, D. A. Wood, C. Brahms, A. Gregory, K. B. Holzner, S. Jarosch, E. W. Larsen, S. Parker, C. S. Strüber, P. Ye, J. W. G. Tisch, and J. P. Marangos, High-flux soft x-ray harmonic generation from ionization-shaped few-cycle laser pulses, Sci. Adv. 4, eaar3761 (2018).
- [12] J. Pupeikis, P.-A. Chevreuil, N. Bigler, L. Gallmann, C. R. Phillips, and U. Keller, Water window soft x-ray source enabled by a 25 W few-cycle 2.2  $\mu$ m OPCPA at 100 kHz, Optica 7, 168 (2020).
- [13] Y. Pertot, C. Schmidt, M. Matthews, A. Chauvet, M. Huppert, V. Svoboda, A. von Conta, A. Tehlar, D. Baykusheva, J.-P. Wolf, and H. J. Wörner, Time-resolved x-ray absorption spectroscopy with a water window high-harmonic source, Science 355, 264 (2017).
- [14] A. R. Attar, A. Bhattacherjee, C. D. Pemmaraju, K. Schnorr, K. D. Closser, D. Prendergast, and S. R. Leone, Femtosecond x-ray spectroscopy of an electrocyclic ring-opening reaction, Science 356, 54 (2017).
- [15] A. Chew, N. Douguet, C. Cariker, J. Li, E. Lindroth, X. Ren, Y. Yin, L. Argenti, W. T. Hill, and Z. Chang, Attosecond transient absorption spectrum of argon at the  $L_{2,3}$  edge, Phys. Rev. A 97, 031407(R) (2018).
- [16] B. Buades, A. Picón, E. Berger, I. León, N. Di Palo, S. L. Cousin, C. Cocchi, E. Pellegrin, J. H. Martin, S. Mañas-Valero, E. Coronado, T. Danz, C. Draxl, M. Uemoto, K. Yabana, M. Schultze, S. Wall, M. Zürch, and J. Biegert, Attosecond state-resolved carrier motion in quantum materials probed by soft x-ray XANES, Appl. Phys. Rev. 8, 011408 (2021).
- [17] N. Saito, H. Sannohe, N. Ishii, T. Kanai, N. Kosugi, Y. Wu, A. Chew, S. Han, Z. Chang, and J. Itatani, Real-time observation of electronic, vibrational, and rotational dynamics in nitric oxide

- with attosecond soft x-ray pulses at 400 eV, Optica 6, 1542 (2019).
- [18] J. Adachi, N. Kosugi, and A. Yagishita, Symmetry-resolved soft x-ray absorption spectroscopy: its application to simple molecules, J. Phys. B: At. Mol. Opt. Phys. **38**, R127 (2005).
- [19] M. Sabbar, H. Timmers, Y.-J. Chen, A. K. Pymer, Z.-H. Loh, S. G. Sayres, S. Pabst, R. Santra, and S. R. Leone, Stateresolved attosecond reversible and irreversible dynamics in strong optical fields, Nat. Phys. 13, 472 (2017).
- [20] C. A. Haworth, L. E. Chipperfield, J. S. Robinson, P. L. Knight, J. P. Marangos, and J. W. G. Tisch, Half-cycle cutoffs in harmonic spectra and robust carrier-envelope phase retrieval, Nat. Phys. 3, 52 (2007).
- [21] P. Saxe, B. H Lengsfield, B. H. R. Martin, and M. Page, MESA (Molecular Electronic Structure Applications), University of California, 1990.
- [22] T. H. Dunning Jr., Gaussian basis sets for use in correlated molecular calculations. I. The atoms boron through neon and hydrogen, J. Chem. Phys. 90, 1007 (1989).
- [23] M. Ehara, T. Horikawa, R. Fukuda, H. Nakatsuji, T. Tanaka, M. Hoshino, H. Tanaka, and K. Ueda, Theoretical spectroscopy of O 1s and N 1s excited states of N<sub>2</sub>O, J. Phys.: Conf. Ser. 288, 012024 (2011).
- [24] M. V. Ammosov, N. B. Delone, and V. P. Krainov, Tunnel ionization of complex atoms and of atomic ions in an alternating electromagnetic field, Sov. Phys. JETP **64**, 1191 (1986).
- [25] P. Hamm, Coherent effects in femtosecond infrared spectroscopy, Chem. Phys. 200, 415 (1995).
- [26] M. Uiberacker, Th. Uphues, M. Schultze, A. J. Verhoef, V. Yakovlev, M. F. Kling, J. Rauschenberger, N. M. Kabachnik, H. Schroder, M. Lezius, K. L. Kompa, H.-G. Muller, M. J. J. Vrakking, S. Hendel, U. Kleineberg, U. Heinzmann, M. Drescher, and F. Krausz, Attosecond real-time observation of electron tunnelling in atoms, Nature (London) 446, 627 (2007).
- [27] E. Goulielmakis, Z.-H. Loh, A. Wirth, R. Santra, N. Rohringer, V. S. Yakovlev, S. Zherebtsov, T. Pfeifer, A. M. Azzeer, M. F. Kling, S. R. Leone, and F. Krausz, Real-time observation of valence electron motion, Nature (London) 466, 739 (2010).
- [28] P. M. Kraus, B. Mignolet, D. Baykusheva, A. Rupenyan, L. Horný, E. F. Penka, G. Grassi, O. I. Tolstikhin, J. Schneider, F. Jensen, L. B. Madsen, A. D. Bandrauk, F. Remacle, and H. J. Wörner, Measurement and laser control of attosecond charge migration in ionized iodoacetylene, Science 350, 790 (2015).
- [29] J. Stöhr, NEXAFS Spectroscopy (Springer, New York, 1992).